

Topological phase transition in layered magnetic compound MnSb_2Te_4 : Spin-orbit coupling and interlayer coupling dependences

Liqin Zhou,^{1,2} Zhiyun Tan,^{3,1} Dayu Yan,^{1,2} Zhong
Fang,^{1,2} Youguo Shi,^{1,2,*} and Hongming Weng^{1,2,4,†}

¹*Beijing National Laboratory for Condensed Matter Physics and Institute of physics,
Chinese academy of sciences, Beijing 100190, China*

²*University of Chinese academy of sciences, Beijing 100049, China*

³*School of Physics and Electronic Science, Zunyi Normal University,
Zunyi 563006, Guizhou, People's Republic of China*

⁴*Songshan Lake Materials Laboratory,
Dongguan, Guangdong 523808, China*

Abstract

Based on the first-principles calculations and theoretical analysis, we investigate the electronic structures, topological phase transition (TPT) and topological properties of layered magnetic compound MnSb_2Te_4 . It has the similar crystal and magnetic structure as the magnetic topological insulator MnBi_2Te_4 . We find that when the spin-orbit coupling (SOC) is considered, the band structure of MnSb_2Te_4 in antiferromagnetic (AFM) state has no band inversion at Γ . This is due to the SOC strength of Sb is less than that of Bi. The band inversion can be realized by increasing the SOC of Sb by 0.3 times, which drives MnSb_2Te_4 from a trivial AFM insulator to an AFM topological insulator (TI) or axion insulator. Uniaxial compressive strain along the layer stacking direction is another way to control the band inversion. The interlayer distance shorten by 5% is needed to drive the similar TPT. For the ferromagnetic (FM) MnSb_2Te_4 with experimental crystal structure, it is a normal FM insulator. The band inversion can happen when SOC is enhanced by 0.1 times or the interlayer distance is decreased by more than 1%. Thus, FM MnSb_2Te_4 can be tuned to be the simplest type-I Weyl semimetal with only one pair of Weyl nodes on the three-fold rotational axis. These two Weyl nodes are projected onto $(1\bar{1}0)$ surface with one Fermi arc connecting them.

I. INTRODUCTION

Topological insulators (TIs) of Z_2 classification protected by time-reversal symmetry is characterized by the gapless topological boundary states with Dirac cone like dispersion. It has attracted intensive studies in the field of condensed matter physics [1–4]. When magnetism is induced into TIs, the gapless topological boundary states are expected to be gapped and various exotic topological phenomena will emerge, including topological magnetoelectric effect [5, 6], axion insulator [7–10] and quantum anomalous hall effect (QAHE) [11–14]. The typical three-dimensional (3D) TIs of Bi_2Te_3 family have provided a fertile field to host many of these exotic phenomena [15, 16], especially the QAHE in (Cr, V)-doped $(\text{Bi, Sb})_2\text{Te}_3$ thin films [12, 17, 18]. Recently, magnetic layered material MnBi_2Te_4 family has been proposed theoretically to be magnetic TI and many experimental studies have immediately performed to confirm this [19–29]. It crystallizes in a layered structure with the $R\bar{3}m$ space group (No.166). Each layer is a septuple layer (SL) composed of “Te-Bi-Te-Mn-Te-Bi-Te” in a triangle lattice [30] and these SLs are stacking through van der Waals interaction. The magnetic ground state of MnBi_2Te_4 is layered AFM state. In each SL, the magnetic moments of Mn ions are pointing out of the plan to form ferromagnetic (FM) ordering, and they are antiparallel to those in the neighboring SLs. When the number of SLs various, the thin film of MnBi_2Te_4 can change from FM (a single SL) to compensated AFM (even number of SLs) and uncompensated AFM (odd number of SLs). Within external field, it is also possibly be tuned to be FM. Therefore, there have been experimental evidences on Chern insulator, axion insulator, AFM TI and type-II Weyl semimetal (WSM) state realized [31] in MnBi_2Te_4 system. The layered crystal structure, layered antiferromagnetic (AFM) configuration and tunable magnetic orders with external magnetic field make it highly attractive in both fundamental research and potential applications.

MnBi_2Te_4 can be viewed as intercalating a Mn-Te bilayer into the center of a Bi_2Te_3 quintuple layer. There arises a question that whether the topological properties can be preserved when we replace Bi_2Te_3 quintuple layer with Sb_2Te_3 , although Sb_2Te_3 is also a 3D strong TI of the same family. However, the spin-orbit coupling (SOC) strength of Sb $5p$ orbitals ($\lambda_{\text{Sb}}=0.4$ eV) is far less than that of Bi $6p$ ones ($\lambda_{\text{Bi}}=1.25$ eV), we would like to study how the topological states of MnSb_2Te_4 are influenced by the SOC and even the interlayer interaction of SLs. In fact, Murakami *et al.* [27] recently have proposed that it is possible to realize FM state in MnSb_2Te_4 due to the mixing of Mn and Sb sites. They also proposed the FM state might be a type-II WSM based on

their calculations. Furthermore, Shi *et al.* [32] have observed anomalous Hall effect in MnSb_2Te_4 , supporting the FM or ferrimagnetic order in MnSb_2Te_4 .

II. METHOD

To obtain the electronic structures of MnSb_2Te_4 , we use the Vienna ab initio simulation package (VASP) with projector augmented wave (PAW) method based on the density functional theory (DFT) [33, 34]. The Perdew-Burke-Ernzerhof (PBE) exchange-correlation functional with GGA+ U method is used to treat the localized $3d$ orbitals of Mn [35]. The cutoff energy for the plane-wave basis is set of 520 eV and the U parameter is selected to be 4 eV for Mn $3d$ orbitals. Spin-orbit coupling (SOC) is included self-consistently and we set the local magnetic moment on Mn ions to be along c -axis. The Brillouin zone (BZ) integral is implemented on a Γ centered grid mesh of $11 \times 11 \times 11$ for self-consistent calculations. The surface states and Fermi arc are calculated by using the WannierTools software package based on the maximally localized Wannier functions (MLWF) [36, 37].

Single crystals of MnSb_2Te_4 were synthesized by using flux method. Starting materials Mn (piece, 99.99%), Sb (grain, 99.9999%) and Te (lump, 99.9999%) were mixed in an Ar-filled glove box at a molar ratio of Mn : Sb : Te = 1 : 10 : 16. The mixture was placed in an alumina crucible, which was then sealed in an evacuated quartz tube. The tube was heated to 700 °C over 10 h and dwelt for 20 h. Then, the tube was slowly cooled down to 630 °C at a rate of 0.5 °C/h followed by separating the crystals from the flux by centrifuging. Shiny crystals with large size were obtained on the bottom of the crucible.

To investigate the crystalline structure, single-crystal x-ray diffraction (XRD) was carried out on Bruker D8 Venture diffractometer at 293 K using Mo $K\alpha$ radiation ($\lambda = 0.71073 \text{ \AA}$). The crystalline structure was refined by full-matrix least-squares method on F^2 by using the SHELXL-2016/6 program. The detailed crystallographic parameters are summarized in Table. I. The single-crystal XRD study revealed that MnSb_2Te_4 have the same structure with MnBi_2Te_4 . The lattice parameters of MnSb_2Te_4 is $a = 4.2613 \text{ \AA}$ and $c = 41.062 \text{ \AA}$, respectively. Fig.1(a) shows the XRD patterns of a flat surface of MnSb_2Te_4 single crystal, where only 00l peaks are detected. A photograph of a typical MnSb_2Te_4 crystal were shown in the inset of Fig.1(b), and the back square of $1 \times 1 \text{ mm}$ indicates the size of the crystal. Though there is mixing of Mn and Sb sites and it might cause the FM state in MnSb_2Te_4 , we take the ideal crystal structure without such mixing in

the calculations. A schematic drawing of the ideal crystal structure based on the experimental one is shown in Fig.1(c). In space group No. 166, symmetric operations mainly include: three-fold rotation symmetry around the z axis C_{3z} , two-fold rotation symmetry around the x and y axis, and inversion symmetry.

III. RESULTS AND DISCUSSIONS

A. AFM state of MnSb_2Te_4

Here, we present and discuss the results of the AFM state firstly. Similar to MnBi_2Te_4 , the layered antiferromagnetic state has six formula units in a conventional unit cell shown in Fig.2(a). The AFM state has a combined symmetrical operation $S \equiv \Theta\tau_{1/2}$, namely time-reversal operator Θ and the translation operator of half unit cell $\tau_{1/2}$ of the AFM lattice. $\tau_{1/2}$ is formed by the nearest neighbor's opposite spin moment of Mn atom layers. According to the GGA+ U calculation, we find that the total energy of AFM state is lower than that of FM state when SOC is considered, which is the same as that in MnBi_2Te_4 [19–21] and consistent with experimental measurements that MnSb_2Te_4 has such layered AFM state. Fig.2(c) and (d) show the band structures of MnSb_2Te_4 for AFM state without and with SOC, respectively. There is a direct gap of about 0.28 eV at Γ point without SOC, but it reduces to about 0.075 eV when SOC is further considered. This means SOC can enhance the band inversion as it does in TIs of Bi_2Te_3 family. Though the magnetism of MnSb_2Te_4 breaks the time reversal symmetry (TRS), the spatial inversion symmetry I and the combined symmetry S are preserved [19, 20, 38]. Therefore, the topological invariant Z_2 protected by S can be obtained through parity configuration or the evolution of hybrid Wannier function centers (WCCs) of occupied states to judge the topological properties of AFM state [2, 39, 40]. The parities of occupied states at Γ point and three equivalent F points $(\pi, \pi, 0)$ indicate that MnSb_2Te_4 is not an AFM TI protected by S , which is consistent with the absence of band inversion at Γ . Since MnBi_2Te_4 is an AFM TI and the SOC strength of Sb $5p$ orbitals is obviously smaller than that of Bi $6p$, we will manipulate λ_{Sb} to demonstrate that SOC can drive the topological phase transition.

The value of Sb p orbitals, which is parameterized as λ_{Sb} , is to be tuned in the self-consistent calculations. As shown in Fig.3(a) and (b), the band structure of MnSb_2Te_4 evolves when λ_{Sb} increases. Those calculated when λ_{Sb} is 1.3 and 1.5 times of its atomic value λ_0 have been plotted.

Obviously, when $\lambda_{Sb}=1.3\lambda_0$, the band gap at Γ closes, which is the critical point of topological phase transition. When $\lambda_{Sb}=1.5\lambda_0$, we find it becomes an AFM TI, the same as MnBi_2Te_4 , which means that band inversion has occurred driven by SOC. According to the critical value of SOC, it is possible to make series of samples $\text{MnSb}_x\text{Bi}_{2-x}\text{Te}_4$ to study the topological phase transition.

In addition to directly adjusting the SOC strength λ_{Sb} in experimental sample synthesizing through alloying Sb and Bi, we try to simulate the topological phase transition by applying pressure or strain to MnSb_2Te_4 . This is another usual way to control the physical properties of solids. We simulate the uniaxial compressive strain along z -axis by decreasing the interlayer distance among septuple layers along c lattice vector. Fig.3(c)-(d) shows the band structures when c is decreased by 5% to 6%. We find that when c is compressed by about 5% the band gap closes and it becomes an AFM TI if further compressed. For the case of 6%, the Z_2 invariant is 1 as shown by the Wilson loop in Fig. 3(e), indicating that the band inversion has occurred at Γ . We calculate the surface states for the case of 6% for the $(1\bar{1}0)$ surface in Fig. 3(f), which is a surface that preserves the symmetry $S=\Theta\tau_{1/2}$ [19, 20]. It is clear to see that there is a Dirac cone like topological surface states in the band gap connecting the conduction and valence band, respectively, though the band gap is quite small that the lower Dirac cone is buried beneath the bulk states. On the contrary, we can only see a trivial gapped surface state on the (111) surface, which does not preserve S symmetry.

B. FM state of MnSb_2Te_4

Now we discuss the results of the FM MnSb_2Te_4 . The electronic structures of FM MnSb_2Te_4 calculated without and with SOC are shown in Fig.4(a) and (b), respectively. There is a direct band gap about 0.21 eV between spin-up and spin-down bands at Γ point when SOC is not included. When SOC is taken into account, the band gap is reduced very much to be about 7.75 meV at the Γ point. This is consistent with the observation in the above that SOC will enhance the band inversion.

To check the topological quantum of FM MnSb_2Te_4 , we calculate the topological indice z_4 using the parity eigenvalue $p_n(\Lambda)$ of occupied states n at eight time-reversal invariant momenta (TRIM) Λ since the inversion symmetry is kept [39, 41]. z_4 is defined as

$$z_4 = \sum_{\Lambda \in \text{TRIM}} \sum_{n \in \text{occ}} \frac{1 + p_n(\Lambda)}{2} \text{mod } 4. \quad (1)$$

If $z_4 = 1, 3$, it means a Weyl semimetal (WSM) phase, where an odd number of Weyl nodes exist in half of the BZ. If $z_4 = 2$, it indicates an axion insulator. The above AFM TI state after tuning can also be looked as an axion insulator. We find that the FM MnSb_2Te_4 with experimental lattice structure is a trivial insulator with full gap throughout the whole BZ with $z_4=0$. The parity eigenvalues of the bands around the Fermi level at Γ have been indicated with “+” or “-” in Fig. 4(b) since only the bands at Γ will have band inversion during the tuning. In order to realize WSM state, we pressurized the FM structure of MnSb_2Te_4 along c axis as done in AFM case. Fig.5(a) and (b) show the calculated bands of FM structure compressed by 1% and 3%, respectively. Through the parity configuration of the bands at Γ , one can immediately find that z_4 changes from 0 to 1, indicating there is odd number of Weyl nodes in half of the BZ. Comparing with the AFM state, 1% compression is enough to drive the topological phase transition and generates cross points, i.e. Weyl nodes. We have searched that the Weyl nodes are on the Γ -Z path, i.e. on the C_{3z} rotation axis. The C_{3z} symmetry is preserved in either AFM or FM states we studied with Mn local magnetic moment pointing parallel to the axis. The inversion symmetry relates the Weyl node in $k_z > 0$ BZ with its pair partner of opposite chirality in $k_z < 0$ BZ. If the Weyl nodes are away from the C_{3z} rotation axis, there will be at least three (odd number) pairs of them in the whole BZ. These Weyl nodes are type-I with upright cones shown in the insets of Fig. 5(a) and (b). We choose the structure under 3% compressive strain to show its Weyl nodes, surface states and Fermi arc. As shown in Fig.5(e), we calculate the $(1\bar{1}0)$ surface. k_z is along the projection line of path Γ -Z of 3D BZ. The two solid Dirac cones close to $\bar{\Gamma}$ near Fermi level are the projections of two Weyl nodes. Their chirality is 1 and -1, respectively, and the energy is very close to the Fermi level ($E_{arc} \approx 0.007\text{eV}$). There are two a very clear surface bands connecting the projections of the two Weyl nodes as depicted in Fig.5(e), and they lead to the Fermi arc connecting the Weyl nodes is also clearly visible in Fig.5(f). These are obvious and typical characterizations of type-I WSM [42–44]. It is known that the insulating electronic state constrained within the two-dimensional plane perpendicular to k_z will have different Chern number C when the plane locates between the two Weyl nodes or out of them as indicated in Fig. 5(f) [45, 46]. This distribution of C is consistent with the number of crossing points between Fermi arc and a reference line in horizontal direction, namely even times (zero or two) in region with $C=0$ and odd times (one) in region with $C=1$.

We also adjust the SOC strength of Sb for the FM state with 1.1 and 1.3 times of the original SOC strength λ_0 and the bands are shown in Fig. 5(c) and (d). Compared with AFM state, it is more prone to emerge topological phase transition for FM state, and 1.1 times of can result in the

occurrence of band inversion and Weyl nodes.

IV. SUMMARY

We mainly investigate the electronic structures, band topology and the surface states for the AFM and FM state of layered magnetic material MnSb_2Te_4 , which has been synthesized experimentally. The dependences of these on the SOC strength and the uniaxial strain have been simulated by first-principles calculations. We find that in the AFM state, the SOC strength of Sb is too small and MnSb_2Te_4 is not an AFM TI. However, the band inversion can be realized when the interlayer distance is decreased by more than 5%, or the SOC strength λ_{Sb} of Sb is increased to more than its 1.3 times. Both can drive topological phase transition and lead MnSb_2Te_4 to AFM TI. In the FM state, MnSb_2Te_4 is not a WSM in its experimental structure. The compressive strain decreasing the interlayer distance by about 1% or increasing λ_{Sb} by about 1.1 times can realize the band inversion, and drive the topological phase transition to WSM. The Weyl nodes appear on the Γ -Z path and they are type-I upright Weyl cone.

This work was supported by the National Natural Science Foundation of China (11504117, 11674369, 11925408, 11974395, 11921004). Z.T. acknowledges the Foundation of Guizhou Science and Technology Department under Grant No. QKH-LHZ[2017]7091. H.W. acknowledges support from the National Key Research and Development Program of China (Grant Nos. 2016YFA0300600 and 2018YFA0305700), the K. C. Wong Education Foundation (GJTD-2018-01), the Beijing Natural Science Foundation (Z180008), and the Beijing Municipal Science and Technology Commission (Z181100004218001).

* ygshi@iphy.ac.cn

† hmweng@iphy.ac.cn

- [1] Liang Fu, Charles L Kane, and Eugene J Mele. Topological insulators in three dimensions. *Physical Review Letters*, 98(10):106803, 2007.
- [2] Liang Fu and Charles L Kane. Topological insulators with inversion symmetry. *Physical Review B*, 76(4):045302, 2007.
- [3] M Zahid Hasan and Charles L Kane. Colloquium: topological insulators. *Reviews of Modern Physics*, 82(4):3045, 2010.

- [4] Xiao-Liang Qi and Shou-Cheng Zhang. Topological insulators and superconductors. *Reviews of Modern Physics*, 83(4):1057, 2011.
- [5] Xiao-Liang Qi, Taylor L Hughes, and Shou-Cheng Zhang. Topological field theory of time-reversal invariant insulators. *Physical Review B*, 78(19):195424, 2008.
- [6] Xiao-Liang Qi, Taylor L Hughes, and Shou-Cheng Zhang. Fractional charge and quantized current in the quantum spin hall state. *Nature Physics*, 4(4):273, 2008.
- [7] Rundong Li, Jing Wang, Xiao-Liang Qi, and Shou-Cheng Zhang. Dynamical axion field in topological magnetic insulators. *Nature Physics*, 6(4):284–288, 2010.
- [8] Nicodemus Varnava and David Vanderbilt. Surfaces of axion insulators. *Physical Review B*, 98(24):245117, 2018.
- [9] Changming Yue, Yuanfeng Xu, Zhida Song, Hongming Weng, Yuan-Ming Lu, Chen Fang, and Xi Dai. Symmetry-enforced chiral hinge states and surface quantum anomalous hall effect in the magnetic axion insulator $\text{Bi}_{2-x}\text{Sm}_x\text{Se}_3$. *Nature Physics*, 15(6):577–581, 2019.
- [10] Yuanfeng Xu, Zhida Song, Zhijun Wang, Hongming Weng, and Xi Dai. Higher-order topology of the axion insulator EuIn_2As_2 . *Physical Review Letters*, 122(25):256402, 2019.
- [11] F Duncan M Haldane. Model for a quantum hall effect without landau levels: Condensed-matter realization of the “parity anomaly”. *Physical Review Letters*, 61(18):2015, 1988.
- [12] Rui Yu, Wei Zhang, Hai-Jun Zhang, Shou-Cheng Zhang, Xi Dai, and Zhong Fang. Quantized anomalous hall effect in magnetic topological insulators. *Science*, 329(5987):61–64, 2010.
- [13] Chao-Xing Liu, Xiao-Liang Qi, Xi Dai, Zhong Fang, and Shou-Cheng Zhang. Quantum anomalous hall effect in $\text{Hg}_{1-y}\text{Mn}_y\text{Te}$ quantum wells. *Physical Review Letters*, 101(14):146802, 2008.
- [14] Kentaro Nomura and Naoto Nagaosa. Surface-quantized anomalous hall current and the magnetoelectric effect in magnetically disordered topological insulators. *Physical Review Letters*, 106(16):166802, 2011.
- [15] Haijun Zhang, Chao-Xing Liu, Xiao-Liang Qi, Xi Dai, Zhong Fang, and Shou-Cheng Zhang. Topological insulators in Bi_2Se_3 , Bi_2Te_3 and Sb_2Te_3 with a single dirac cone on the surface. *Nature physics*, 5(6):438, 2009.
- [16] YL Chen, James G Analytis, J-H Chu, ZK Liu, S-K Mo, Xiao-Liang Qi, HJ Zhang, DH Lu, Xi Dai, Zhong Fang, et al. Experimental realization of a three-dimensional topological insulator, Bi_2Te_3 . *Science*, 325(5937):178–181, 2009.

- [17] Cui-Zu Chang, Jinsong Zhang, Xiao Feng, Jie Shen, Zuocheng Zhang, Minghua Guo, Kang Li, Yunbo Ou, Pang Wei, Li-Li Wang, et al. Experimental observation of the quantum anomalous hall effect in a magnetic topological insulator. *Science*, 340(6129):167–170, 2013.
- [18] Cui-Zu Chang, Weiwei Zhao, Duk Y Kim, Haijun Zhang, Badih A Assaf, Don Heiman, Shou-Cheng Zhang, Chaoxing Liu, Moses HW Chan, and Jagadeesh S Moodera. High-precision realization of robust quantum anomalous hall state in a hard ferromagnetic topological insulator. *Nature Materials*, 14(5):473, 2015.
- [19] Jiaheng Li, Yang Li, Shiqiao Du, Zun Wang, Bing-Lin Gu, Shou-Cheng Zhang, Ke He, Wenhui Duan, and Yong Xu. Intrinsic magnetic topological insulators in van der waals layered MnBi_2Te_4 -family materials. *Science Advances*, 5(6):eaaw5685, 2019.
- [20] Dongqin Zhang, Minji Shi, Tongshuai Zhu, Dingyu Xing, Haijun Zhang, and Jing Wang. Topological axion states in the magnetic insulator MnBi_2Te_4 with the quantized magnetoelectric effect. *Physical Review Letters*, 122(20):206401, 2019.
- [21] MM Otrokov, II Klimovskikh, H Bentmann, D Estyunin, A Zeugner, ZS Aliev, S Gaß, AUB Wolter, AV Koroleva, AM Shikin, et al. Prediction and observation of an antiferromagnetic topological insulator. *Nature*, 576(7787):416–422, 2019.
- [22] Sugata Chowdhury, Kevin F Garrity, and Francesca Tavazza. Prediction of weyl semimetal and antiferromagnetic topological insulator phases in Bi_2MnSe_4 . *npj Computational Materials*, 5(1):33, 2019.
- [23] SV Eremeev, MM Otrokov, and Eugene V Chulkov. Competing rhombohedral and monoclinic crystal structures in MnPn_2Ch_4 compounds: An ab-initio study. *Journal of Alloys and Compounds*, 709:172–178, 2017.
- [24] MM Otrokov, IP Rusinov, M Blanco-Rey, M Hoffmann, A Yu Vyazovskaya, SV Eremeev, A Ernst, PM Echenique, A Arnau, and EV Chulkov. Unique thickness-dependent properties of the van der waals interlayer antiferromagnet MnBi_2Te_4 films. *Physical Review Letters*, 122(10):107202, 2019.
- [25] J-Q Yan, Satoshi Okamoto, Michael A McGuire, Andrew F May, Robert John McQueeney, and Brian C Sales. Evolution of structural, magnetic, and transport properties in $\text{MnBi}_{2-x}\text{Sb}_x\text{Te}_4$. *Physical Review B*, 100(10):104409, 2019.
- [26] Przemyslaw Swatek, Yun Wu, Lin-Lin Wang, Kyungchan Lee, Benjamin Schruck, Jiaqiang Yan, and Adam Kaminski. Gapless dirac surface states in the antiferromagnetic topological insulator MnBi_2Te_4 . *arXiv preprint arXiv:1907.09596*, 2019.

- [27] Taito Murakami, Yusuke Nambu, Takashi Koretsune, Gu Xiangyu, Takafumi Yamamoto, Craig M Brown, and Hiroshi Kageyama. Realization of interlayer ferromagnetic interaction in MnSb_2Te_4 toward the magnetic weyl semimetal state. *Physical Review B*, 100(19):195103, 2019.
- [28] Yang Li, Zeyu Jiang, Jiaheng Li, Shengnan Xu, and Wenhui Duan. Magnetic anisotropy of the two-dimensional ferromagnetic insulator MnBi_2Te_4 . *Physical Review B*, 100(13):134438, 2019.
- [29] Hang Li, Shun-Ye Gao, Shao-Feng Duan, Yuan-Feng Xu, Ke-Jia Zhu, Shang-Jie Tian, Jia-Cheng Gao, Wen-Hui Fan, Zhi-Cheng Rao, Jie-Rui Huang, et al. Dirac surface states in intrinsic magnetic topological insulators EuSn_2As_2 and $\text{MnBi}_{2n}\text{Te}_{3n+1}$. *Physical Review X*, 9(4):041039, 2019.
- [30] Dong Sun Lee, Tae-Hoon Kim, Cheol-Hee Park, Chan-Yeup Chung, Young Soo Lim, Won-Seon Seo, and Hyung-Ho Park. Crystal structure, properties and nanostructuring of a new layered chalcogenide semiconductor, Bi_2MnTe_4 . *CrystEngComm*, 15(27):5532–5538, 2013.
- [31] Seng Huat Lee, Yanglin Zhu, Hemian Yi, David Graf, Rabindra Basnet, Arash Fereidouni, Aaron Wegner, Yi-Fan Zhao, Lujin Min, Katrina Verlinde, et al. Transport evidence for a magnetic-field induced ideal weyl state in antiferromagnetic topological insulator MnBi_2Te_4 . *arXiv preprint arXiv:2002.10683*, 2020.
- [32] Gang Shi, Mingjie Zhang, Dayu Yan, Honglei Feng, Meng Yang, Youguo Shi, and Yongqing Li. Anomalous hall effect in layered ferrimagnet MnSb_2Te_4 . *Chinese Physics Letters*, 37(4):047301, 2020.
- [33] Georg Kresse and Jürgen Furthmüller. Efficient iterative schemes for ab initio total-energy calculations using a plane-wave basis set. *Physical Review B*, 54(16):11169, 1996.
- [34] Georg Kresse and Daniel Joubert. From ultrasoft pseudopotentials to the projector augmented-wave method. *Physical Review B*, 59(3):1758, 1999.
- [35] John P Perdew, Kieron Burke, and Matthias Ernzerhof. Generalized gradient approximation made simple. *Physical Review Letters*, 77(18):3865, 1996.
- [36] QuanSheng Wu, ShengNan Zhang, Hai-Feng Song, Matthias Troyer, and Alexey A Soluyanov. Wanniertools: An open-source software package for novel topological materials. *Computer Physics Communications*, 224:405–416, 2018.
- [37] Arash A Mostofi, Jonathan R Yates, Young-Su Lee, Ivo Souza, David Vanderbilt, and Nicola Marzari. wannier90: A tool for obtaining maximally-localised wannier functions. *Computer Physics Communications*, 178(9):685–699, 2008.

- [38] Roger SK Mong, Andrew M Essin, and Joel E Moore. Antiferromagnetic topological insulators. *Physical Review B*, 81(24):245209, 2010.
- [39] Ari M Turner, Yi Zhang, Roger SK Mong, and Ashvin Vishwanath. Quantized response and topology of magnetic insulators with inversion symmetry. *Physical Review B*, 85(16):165120, 2012.
- [40] Rui Yu, Xiao Liang Qi, Andrei Bernevig, Zhong Fang, and Xi Dai. Equivalent expression of Z_2 topological invariant for band insulators using the non-abelian berry connection. *Physical Review B*, 84(7):075119, 2011.
- [41] Yuanfeng Xu, Luis Elcoro, Zhida Song, Benjamin J Wieder, MG Vergniory, Nicolas Regnault, Yulin Chen, Claudia Felser, and B Andrei Bernevig. High-throughput calculations of antiferromagnetic topological materials from magnetic topological quantum chemistry. *arXiv*, pages arXiv–2003, 2020.
- [42] Hongming Weng, Chen Fang, Zhong Fang, B Andrei Bernevig, and Xi Dai. Weyl semimetal phase in noncentrosymmetric transition-metal monophosphides. *Physical Review X*, 5(1):011029, 2015.
- [43] Su-Yang Xu, Ilya Belopolski, Nasser Alidoust, Madhab Neupane, Guang Bian, Chenglong Zhang, Raman Sankar, Guoqing Chang, Zhujun Yuan, Chi-Cheng Lee, et al. Discovery of a weyl fermion semimetal and topological fermi arcs. *Science*, 349(6248):613–617, 2015.
- [44] BQ Lv, HM Weng, BB Fu, XP Wang, Hu Miao, Junzhang Ma, P Richard, XC Huang, LX Zhao, GF Chen, et al. Experimental discovery of weyl semimetal TaAs. *Physical Review X*, 5(3):031013, 2015.
- [45] Gang Xu, Hongming Weng, Zhijun Wang, Xi Dai, and Zhong Fang. Chern semimetal and the quantized anomalous hall effect in HgCr_2Se_4 . *Physical Review Letters*, 107(18):186806, 2011.
- [46] Hongming Weng, Rui Yu, Xiao Hu, Xi Dai, and Zhong Fang. Quantum anomalous hall effect and related topological electronic states. *Advances in Physics*, 64(3):227–282, 2015.

Table I. Crystallographic data of MnSb_2Te_4 .

atom	x	y	z	Occ.	Wyckoff Position	Sym.
Mn1	0.00000	1.00000	0.50000	0.680	3b	-3m
Sb1	0.00000	1.00000	0.50000	0.320	3b	-3m
Te1	0.33333	0.66667	0.45887	1	6c	3m
Mn2	0.66667	0.33333	0.40824	0.172	6c	3m
Sb2	0.66667	0.33333	0.40824	0.828	6c	3m
Te2	1.00000	0.00000	0.36864	1	6c	3m

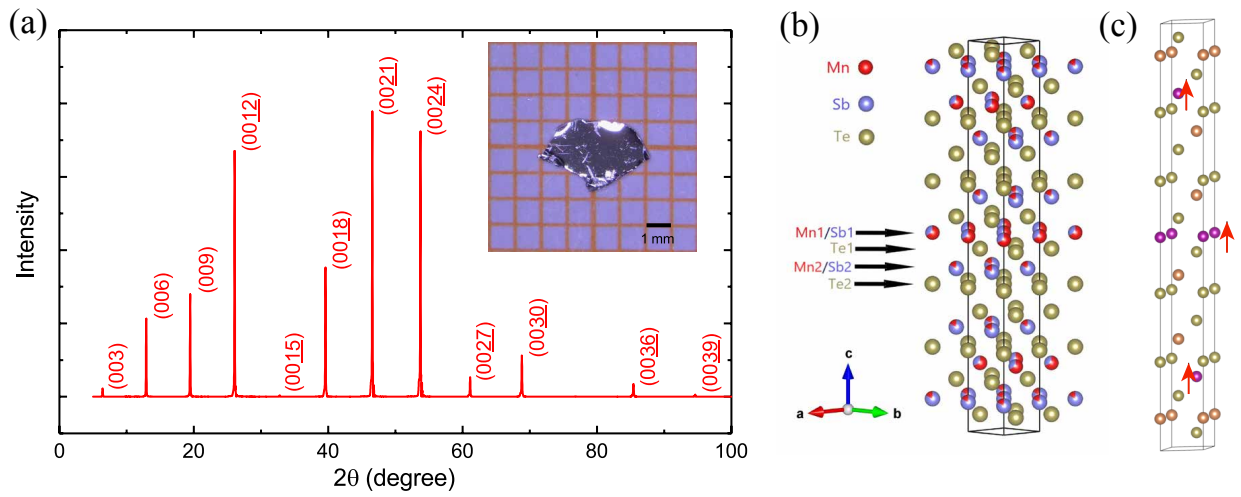


Figure 1. (a) The X-ray diffraction pattern of a flat surface of MnSb_2Te_4 single crystal. The inset shows a photograph of a typical MnSb_2Te_4 single crystal. (b) The schematic crystalline structure of MnSb_2Te_4 from experiment with Mn and Sb site mixing. (c) The schematic drawing of the ideal crystal structure for MnSb_2Te_4 without mixing of Mn and Sb sites. The arrows around Mn indicate the local magnetic moment on it.

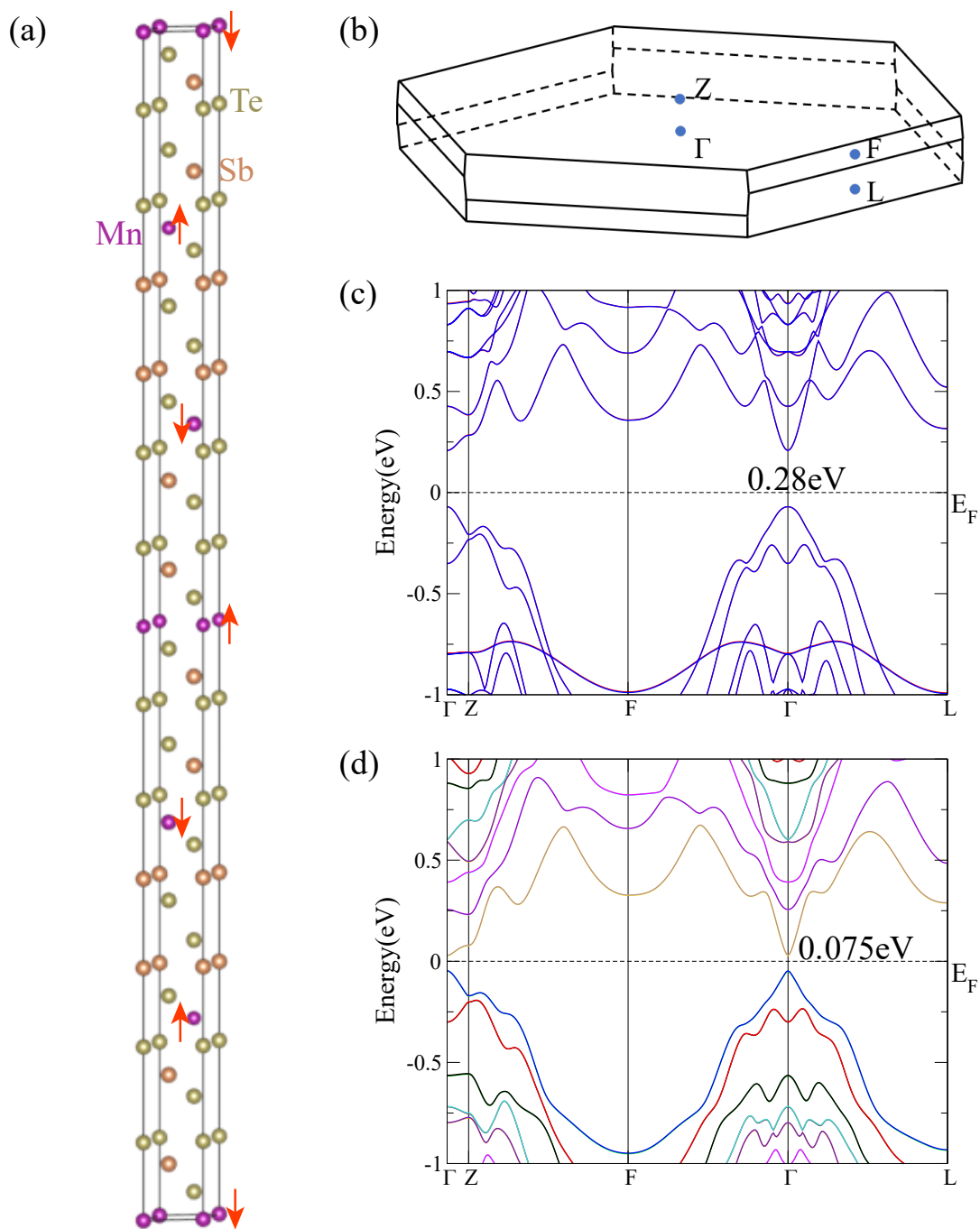


Figure 2. Crystal structure and electronic structure of AFM MnSb₂Te₄. (a) The unit cell of AFM MnSb₂Te₄ and the red arrows represent the spin moment of Mn atom. (b) The first Brillouin zone and four inequivalent TRIM points of MnSb₂Te₄. (c) and (d) The band structure of AFM state without (c) and with (d) SOC.

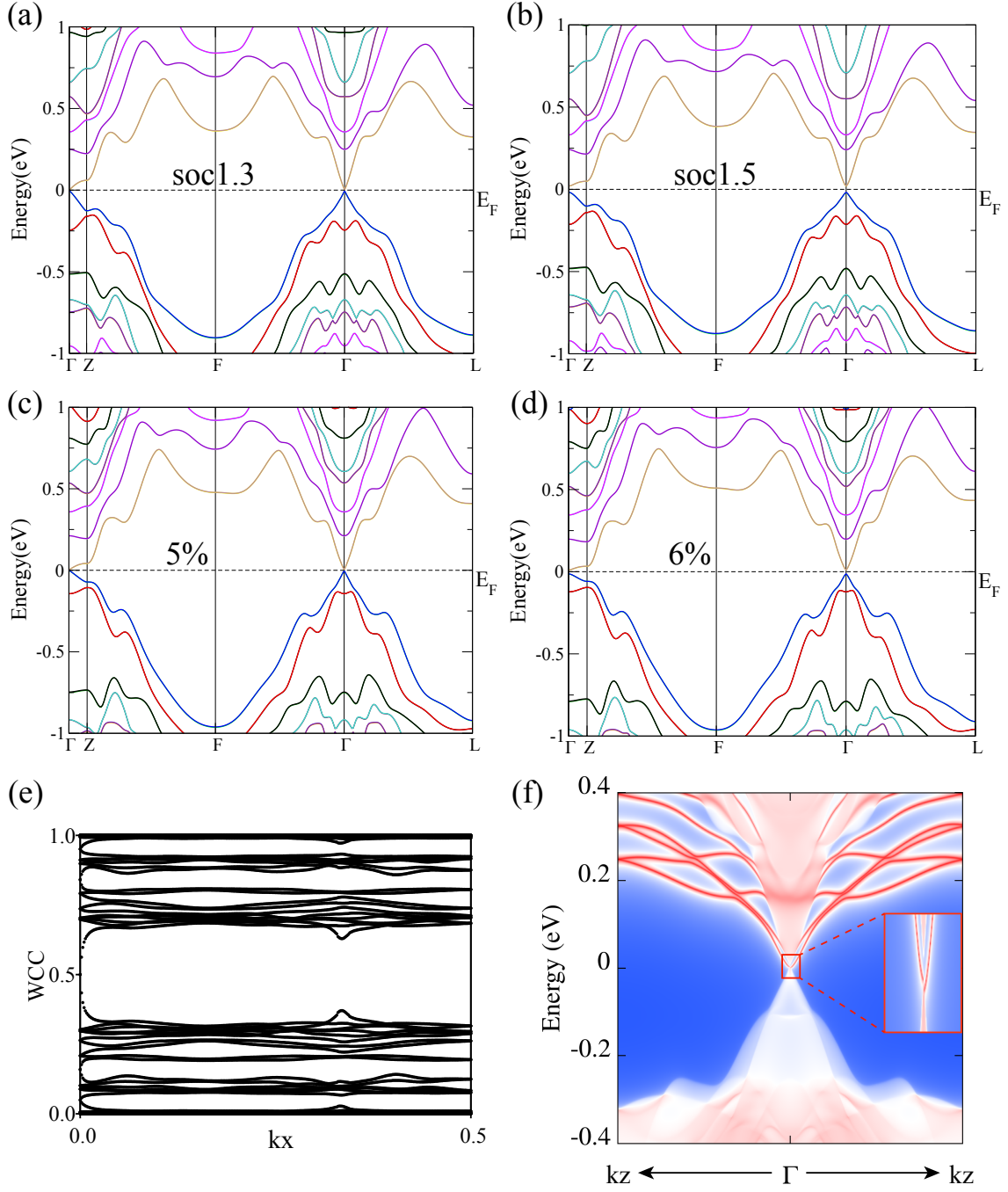


Figure 3. The electronic structures of AFM MnSb₂Te₄ under different conditions. (a) and (b) Band structures for SOC strength λ_{Sb} of Sb changes to 1.3 times and 1.5 times of the original value, respectively. (c) and (d) The band structure with interlayer distance decreased by 5% and 6% along z axis with SOC, respectively. (e) Evolution of WCCs in the $k_z = 0$ plane of AFM MnSb₂Te₄ under 6% compressive strain. It implies a nonzero topological invariant. (f) The surface states on the $(1\bar{1}0)$ surface. The Dirac cone like surface bands are zoomed out around $\bar{\Gamma}$.

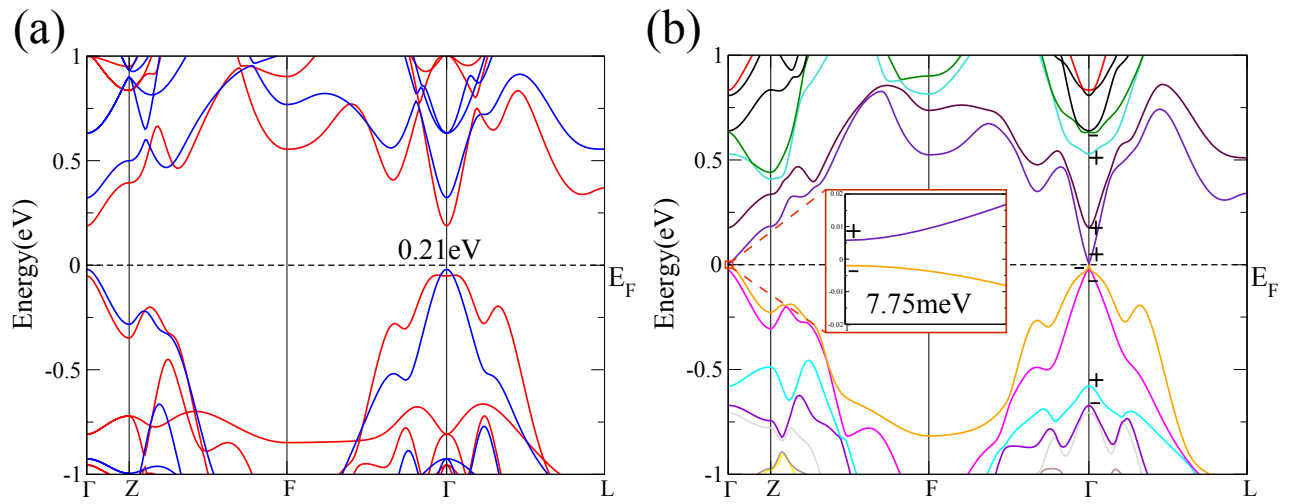


Figure 4. The electronic structures of FM MnSb_2Te_4 . (a) and (b) The band structures of FM state without (a) and with (b) SOC (red bands indicate spin up and blue bands indicate spin down in a).

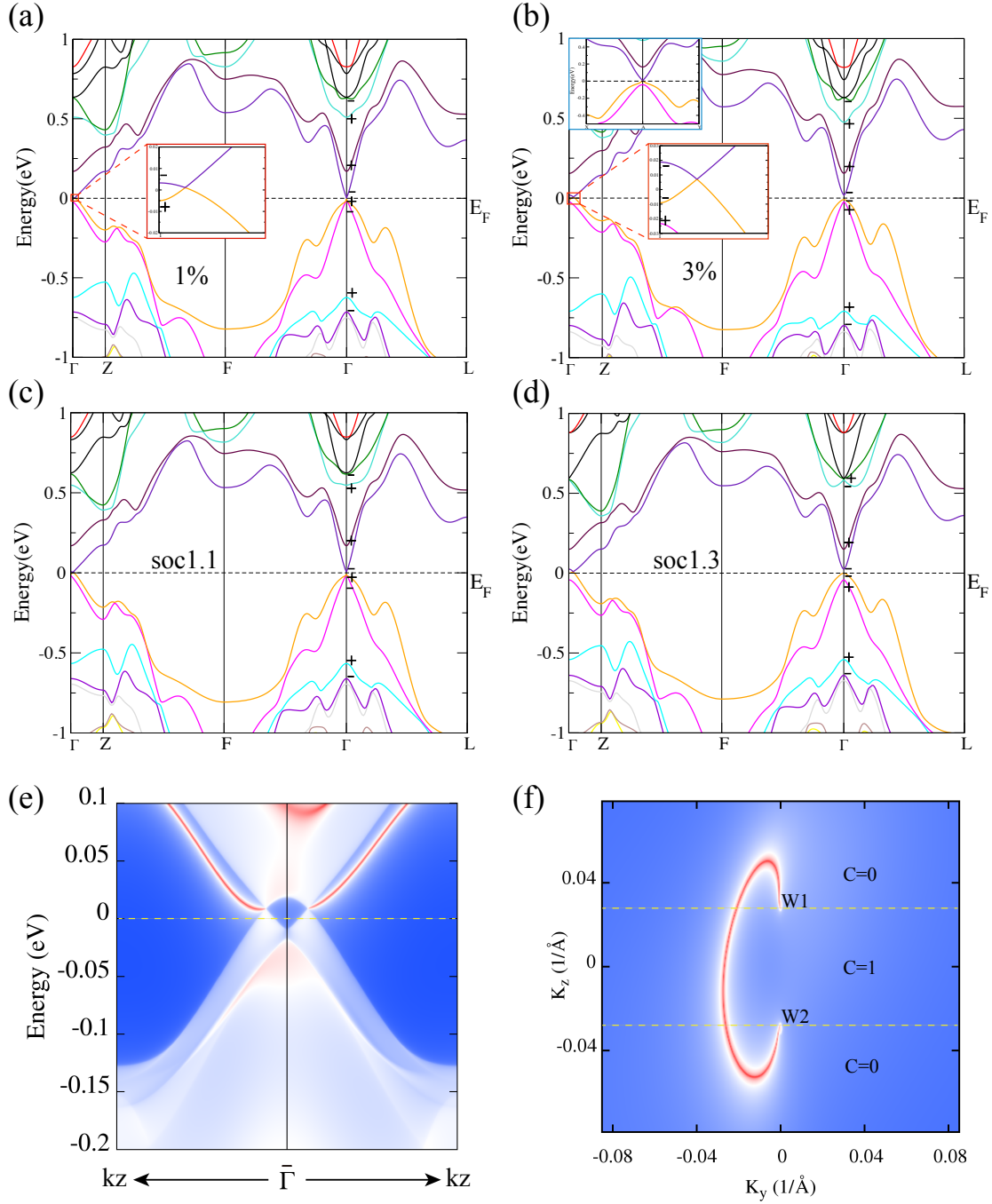


Figure 5. The electronic structures of FM MnSb_2Te_4 under different conditions. (a) and (b) The band structures with interlayer distances decreased by 1% and 3% with SOC, respectively. (The insert of blue border shows the bands along the k_x and k_y axis through the Weyl point in b, which indicates a type-I Weyl point) (c) and (d) Band structures for SOC strength λ_{Sb} of Sb changes to 1.1 and 1.3 times of the original value, respectively. (e) Surface state for case with 3% compressive strain on the $(1\bar{1}0)$ surfaces. There are two Weyl nodes along the k_z direction. (f) Fermi arc connecting the projections of the Weyl nodes W1 and W2 at 0.007 eV.